Low-inductance gas switches for linear transformer drivers

J. R. Woodworth,[1] J. A. Alexander,[1] F. R. Gruner,[4] W. A. Stygar,[1] M. J. Harden,[2] J. R. Blickem,[3] G. J. Dension,[1] F. E. White,[3] L. M. Lucero,[3] H. D. Anderson,[2] L. F. Bennett,[1] S. F. Glover,[1] D. Van DeValde,[5] and M. G. Mazarakis[1]

[1]*Sandia National Laboratories, Albuquerque, New Mexico 87185, USA*
[2]*NSTech Corporation, Los Alamos, New Mexico 87544, USA*
[3]*Ktech Corporation, Albuquerque, New Mexico 87123, USA*
[4]*Kinetech LLC, The Dalles, Oregon 97058, USA*
[5]*EG&G Technical Services, Albuquerque, New Mexico 87119, USA*

(Received 5 February 2009; published 8 June 2009)

We are investigating several alternate gas-switch designs for use in linear transformer drivers. To meet linear-transformer-driver (LTD) requirements, these air-insulated switches must be DC charged to 200 kV, be triggerable with a jitter of 5 ns or less, have very low prefire and no-fire rates (~ 1 in 10^4 shots), and have a lifetime of at least several thousand shots. Since the switch inductance plays a significant role in limiting the rise time and peak current of the LTD circuit, the inductance needs to be as low as possible. The switches are required to conduct current pulses with ~100-ns rise times and 20–80 kA peak currents, depending on the application. Our baseline switch, designed by the High Current Electronics Institute in Tomsk, Russia, is a six-stage switch with an inductance on the order of 115 nH that is insulated with 47–67 psia of air. We are also testing three smaller two-stage switches that have inductances on the order of 66–100 nH. The smaller switches are insulated with 92–252 psia of air.

DOI: 10.1103/PhysRevSTAB.12.060401 PACS numbers: 84.70.+p, 84.32.Ff, 52.80.Mg

I. INTRODUCTION

Linear transformer drivers are a developing pulsed-power architecture that may dramatically reduce the size and cost of high-voltage, high-current pulsed-power accelerators [1–6]. Linear transformer drivers, however, place stringent demands on gas switches, requiring gas switches that can be DC charged to ~200 kV, triggered with ~5–10-ns one sigma jitter [7], be low inductance, have very low prefire and no-fire rates, and have lifetimes of at least several thousand shots. Multi-mega-volt, multi-mega-ampere LTD drivers for controlled fusion, dynamic materials experiments, or flash radiography applications may require as many as 100 000 gas switches [8]. Hence, it is essential that these switches be very reliable.

Linear transformer drivers can potentially achieve compactness and low cost by going directly from DC-charged capacitors to a 100-ns pulse propagating on a vacuum or water transmission line, without any of the pulse-compression sections normally associated with large pulse-power drivers [9–15]. The basic building block of an LTD system called a ''brick'' typically consists of two capacitors, a triggered switch, toroidal rings of magnetic material, and a magnetically insulated transmission line (MITL) [16] in vacuum. Figure 1 shows a typical LTD brick. Two capacitors are charged to opposite polarities with a gas switch between their high-voltage outputs. When the switch is triggered and conducts current, a voltage pulse is induced on the opposite ends of the capacitors. This voltage pulse attempts to drive current around a loop formed by the metallic case of the LTD brick. The toroidal magnetic cores, however, block current from flowing in this loop until the magnetic cores saturate. The result is that a large, fast-rising voltage pulse is impressed on the magnetically insulated transmission line in the center of the vacuum section. Losses in the toroidal cores can reduce the peak power seen at the load by 10%–20% depending on the details of the system. In order to induce a voltage pulse on the MITL with a ~70-ns or less rise time, the inductance of the capacitors, the switch, and the transmission line leading to the vacuum section must be minimized. For example, if two 40 nF capacitors are used in the brick, the inductance of the capacitors, switch, and leads must be no more than 245 nH to achieve a zero-to-peak rise time of 70 ns into a matched load.

Normally, multiple bricks are stacked in parallel around a central vacuum transmission line to form an LTD cavity.

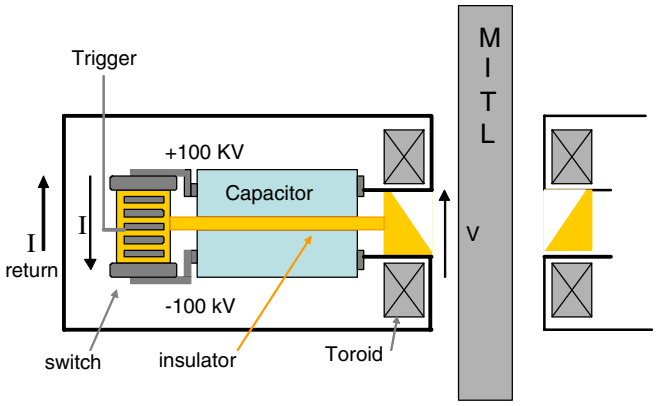

FIG. 1. (Color) Schematic of basis LTD brick driving MITL cavity.

FIG. 2. (Color) LTD-II cavity at Sandia National Laboratories.

Figure 2 shows a picture of an LTD cavity at Sandia Laboratories designed by the High Current Electronics Institute at Tomsk. This cavity has 20 bricks, each containing two 40-nF capacitors and a switch, stacked around a central vacuum cavity. In this picture, the vacuum cavity has been replaced by a liquid resistive load. The cavity generates a 500 kA, 100 kV power pulse across the liquid resistor with a rise time of less than 100 ns. Multiple cavities can then be stacked in series [3,8], to generate voltages above 1 MV.

LTD systems at Sandia Laboratories to date have used gas switches designed by the High Current Electronics Institute [17] in Tomsk, Russia. These switches have been previously described in the literature [4,17]. Figure 3 shows a photograph of one switch used in Sandia's LTDR facility [5] and in Sandia's LTD-II cavity [18]. These switches have six ~6-mm wide high-voltage gaps that are insulated by dry air. Each electrode is a toroidal ring. This toroidal shape of the electrodes allows multiple breakdown arcs in each switch to spread over a large diameter, which lowers the overall inductance of the switch. When submerged in oil, the top and bottom of the switch can be DC charged to plus and minus 100 kV. The center electrode, which functions as the trigger electrode, is held at ground. Corona-discharge stabilization is used to properly grade the voltage across the six gaps. Only four gaps are visible in Fig. 3. The other two gaps are obscured by the top and bottom plates of the switch. This switch has a demonstrated lifetime in excess of 10 000 shots [19] and a command jitter of less than 5 ns one sigma. The relatively large physical size of this switch (~ 16-cm long) means that this switch adds about 115 nH of inductance to an LTD brick circuit. Since this is roughly half the total inductance budget for a brick with 40-nF capacitors that has a rise time of 70 ns, we are investigating a variety of switches that have lower inductances.

FIG. 3. (Color) Russian switch designed by the High Current Electronics Institute attached to capacitors in our LTD brick.

II. APPARATUS

A. Switch-testing apparatus

Figure 4 shows a schematic of our LTD switch-testing apparatus. Our LTD brick has two 40 nF capacitors that are connected to the top and bottom of the test gas switch. The capacitors can be DC charged to plus and minus 100 kV. The other ends of the capacitors would normally be coupled to a vacuum transmission line cavity. In our experiments, however, the other ends of the capacitors are connected simply to each other through a liquid resistive load. A common potassium-bromide solution flowed through both halves of the resistive load to provide the power dissipation capability needed for automated switch lifetime testing. For most of the experiments, the resistance of both halves of the flowing load in series ranged from 2.7 to 3.1 Ohms. A 1-milli-Ohm current-viewing resistor was placed between the two halves of the flowing load to monitor the current in the circuit. A resistive divider monitored voltage across one of the resistive loads to allow us to verify that the value of the resistive loads had not shifted. As indicated in Fig. 1, the brick is ''wrapped'' top, bottom, and ends in a ground plane that simulates the exterior of an LTD cavity. The entire apparatus is submerged in a tank filled with transformer oil for all of the experiments.

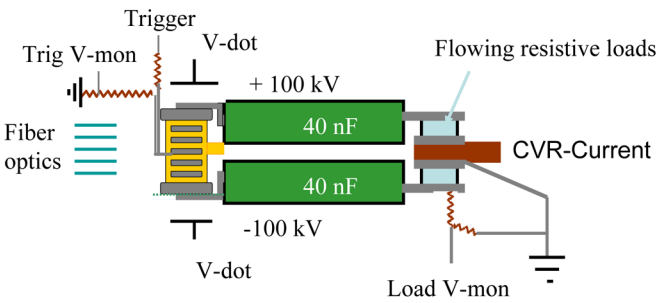

FIG. 4. (Color) Schematic of our LTD brick and diagnostics.

A positive electrical trigger was applied to the midplane of the switch being tested to trigger it. The trigger pulse was a nominal 120 kV pulse with an 8-ns rise time at the trigger generator. A trigger resistor was placed between the trigger generator and the 200-kV switch to protect the trigger generator. Since the value of this trigger resistor could affect the trigger voltage reaching the switch, we also had a 5.1-kiloOhm resistive divider to monitor the trigger voltage at the switch. Capacitive voltage monitors located just above and below the switch end plates measured the voltage across the switch during the discharges. The dV/dt signals from these monitors were ''hard integrated'' with RC integrators. Electrically induced damage to the integrators stopped use of these monitors part way through the experiments. A number of fiber optics leading to photomultiplier tubes were apertured to look at individual gaps in the switches to determine breakdown timing of individual gaps. For some of the tests, a framing camera with a maximum resolution of 5-ns per frame took pictures of the switches during the breakdown process. The entire switch-testing apparatus was controlled by computer to test switches in an automated mode at approximately two shots per minute during switch lifetime testing.

For most of our experiments, the two capacitors in our brick were nominal 40 nF ($\pm$ 10%) capacitors rated for 100-kV use in transformer oil [20]. For the Russian and Sandia switches, some experiments were also performed with two 20 nF capacitors in the brick. All of the results we present, however, are for the 40 nF capacitors unless we specifically state otherwise.

We measured the characteristics of our 40-nF capacitors with a vector impedance meter and obtained measured values of capacitance, series inductance, and series resistance of 38 nF, 16 nH, and 0.1 Ohms, respectively. The two capacitors in series in our brick therefore had effective capacitance and inductance values of 19 nF and 32 nH. Thus, in the absence of any other inductances in the system, our two-capacitor LC system would have a ringing period of ~154 ns and a zero-to-peak current rise time of 39 ns (25 ns 10%–90%). This places an absolute lower limit on our rise times due to the capacitors themselves. Other inductances in the system will make the rise times longer than 39 ns.

B. Switches

Figure 5 shows a photograph of the four switches we tested. Table I summarizes the physical parameters of each switch. The baseline switch designed by the High-Current Electronics Institute (HCEI) has been described above. The switch is 16-cm tall. This switch has the disadvantage of being relatively high inductance (~ 115 nH) due to its relatively large size. It also requires extensive conditioning—more than 100 shots at less than full charge—before it will operate reliably at the full $\pm$100 kV charge voltage. The HCEI switch has the advantage, however, that it is relatively easy to trigger since the trigger pulse only needs to break down one of the six gaps to trigger the switch. All the other switches are two-gap switches and, hence, require a higher-voltage trigger pulse. The HCEI switch also has demonstrated lifetimes in excess of 10 000 shots at a 200 kV charge voltage and ~24 kA peak currents. Gas inlet and outlets are built into the trigger electrode, which is at DC ground. The exterior envelope of this switch is normally fabricated of Caprilon, which is similar to nylon. We used an envelope of polished polycarbonate to allow detailed optical diagnostics of the switch. The end plates and electrodes of the switch are all fabricated of stainless steel. The HCEI switch operates at a relatively low dry air pressure of 52–62 psia.

Detailed pictures of the switch designed at Sandia Laboratories are shown in Fig. 6. This figure shows two views of the switch, on the right is the complete switch. On the left is the switch with its central field-grading torus removed. This switch is designed to minimize its overall

FIG. 5. (Color) Side-by side comparison of the four gas switches tested in these experiments.

TABLE I. Gas switch physical parameters.

Switches	HCEI	Sandia	Kinetech	L3
Gaps	six each 6 mm	two each 12 mm	two each 5 mm	two each 12 mm
Air pressure	57 psia	130 psia	242 psia	72 psia

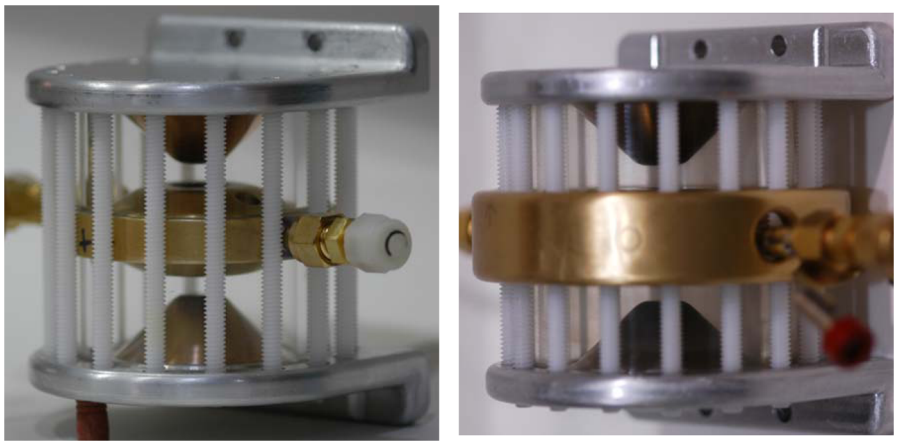

FIG. 6. (Color) Two views of the Sandia-designed switch. The brass doughnut outside the midplane was added to smoothly grade the electric fields around the outer edges of the midplane.

inductance. The 9.2-cm tall switch has a diameter of 10.2 cm and is designed to bolt directly onto the ends of the capacitors. The top and bottom electrodes and the midplane electrode are all conical to minimize the switch's inductance. There are two 12-mm gaps in the switch that are normally insulated with ~130 psia of dry air.

The midplane electrode, which serves both as the trigger electrode and the location of the gas inlets and outlets, has a 1.2-cm diameter hole in the center to allow UV coupling from one gap to the other. The brass midplane electrode has copper-tungsten alloy inserts in its center to maximize the switch's lifetime. The top and bottom electrodes are also fabricated of copper-tungsten alloy. The envelope of the switch is acrylic, the rods holding the switch together are Delrin^{TM} (polyoxymethylene), which is a nonporous plastic that does not swell when it is submerged in water or oil, and the end plates are aluminum. Figure 7 shows a plot of the electric fields in the Sandia switch. When the switch is charged to plus and minus 100 kV, the peak electric field between the electrodes is approximately 190 kV/cm.

Figure 8 shows a cross-sectional drawing of the switch designed by Kinetech LLC and Sandia Labs. This switch is built both for low inductance and for mechanical robustness. The distance between electrodes can be varied by screwing the end pieces in and out along the threads in the main outer "barrel." Since we wanted the lowest possible inductance configuration, we use the switch with the threads screwed in as far as possible. In this configuration, the switch has a diameter of 7.5 cm and is 12 cm long. The end caps of the switch are clamped in split rings that bolt directly to the ends of the capacitors. This switch has two hemispherical electrodes with a 0.95-cm spacing. Four trigger pins are used instead of one because there were concerns that erosion of the trigger pins would limit the lifetime of this switch. The four 0.3-cm diameter trigger pins extend inward from the midplane of the housing towards the center of the switch. The gap between each trigger pin and the main electrodes is 0.5 cm.

Since the discharge normally occurs from one electrode to a trigger pin and then from the trigger pin to the other electrode, the switch effectively has two 0.5-cm gaps. The gas inlet and outlet ports are also on the midplane of the switch as shown in Fig. 8. Figure 9 shows an electrostatic field plot of the Kinetech switch with 200 kV between the

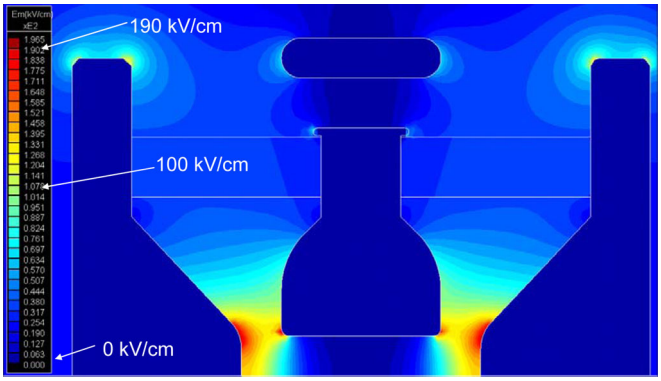

FIG. 7. (Color) Electric fields lines inside the Sandia-designed switch. The peak electric field on both the electrodes and the midplane is 190 kV/cm.

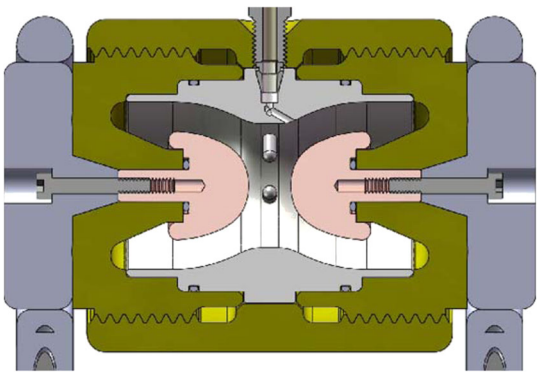

FIG. 8. (Color) Cross-sectional view of the gas switch designed by Kinetech, LLC.

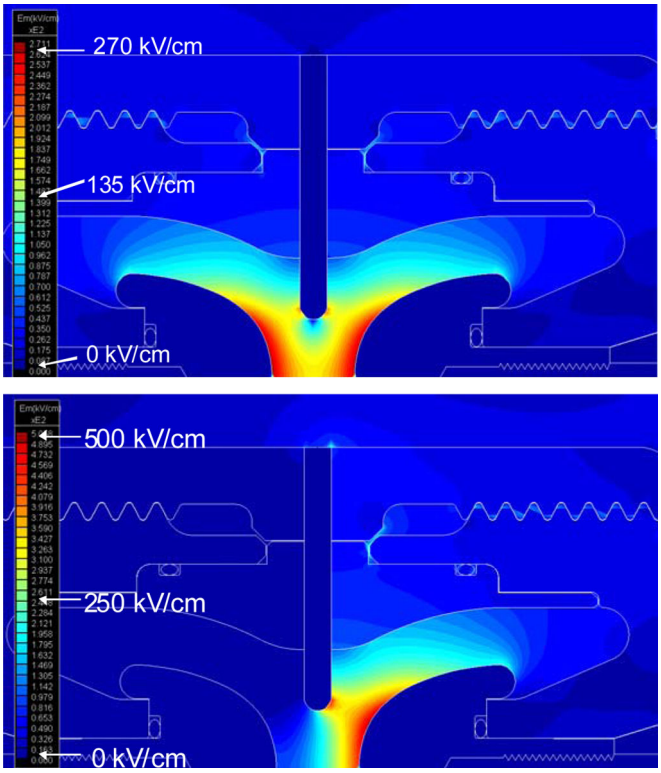

FIG. 9. (Color) Electric field intensities inside Kinetech switch when charged to ±100 kV. Upper picture—DC charge with trigger pins at ground. Lower picture—fields in the switch when the trigger pins are at +100 kV during the triggering process.

electrodes. For this two-dimensional simulation, the trigger pins have been approximated as an annular sheet on the switch midplane. The maximum electric field at the surface of the electrodes is 270 kV/cm. Figure 9 also shows an electrostatic field plot of this switch with the trigger pin at +100 kV as the trigger pulse arrives at the switch. The peak electric field in the switch is now slightly over 500 kV/cm. The outer (brown) insulators are a glass-fiber loaded ULTEM™ plastic and the inner liner is Kel-F™ plastic. The electrodes are a copper-tungsten alloy, the trigger pins are pure tungsten, and the end pieces are an aluminum alloy. It is necessary to vacuum impregnate the exterior of this switch in transformer oil after it is assembled and sealed off. This prevents air gaps in the internal screw threads from providing a low breakdown path from one end cap to the other.

Figure 10 shows a picture of the two halves of the ±100 kV switch purchased from L3-Communications, Pulse Sciences Division [21]. This switch is 14.6-cm in diameter, 7.6-cm tall, and has a cast polycarbonate body [22]. It is a modified version of the L3 ±50 kV switch [23]. The switch has 3-cm diameter flat brass anode and cathode electrodes as shown on the right of Fig. 10 and a solid brass midplane electrode between them shown on the left. Spacing from the anode or cathode to the midplane electrode is 1.2 cm. The midplane electrode has a 0.9-cm central hole to allow UV coupling between the two halves of the switch. The switch also has a UV-preillumination gap in the center of the hole in the midplane. The trigger pulse is forced to pass through a short air arc in the center of the switch in order to reach the midplane. This arc floods the switch interior with UV light as the trigger pulse arrives, improving the triggering. In order to minimize inductance, we connected the capacitors to the L3 switch with triangular current contacts that were 7.6-cm wide at the capacitors and narrowed to 2.5-cm wide on the top and bottom of the switch. In this configuration, we found it necessary to vacuum impregnate the exterior of this switch in oil to prevent air spaces around the insulating bolts from providing a breakdown path between the end plates and the midplane.

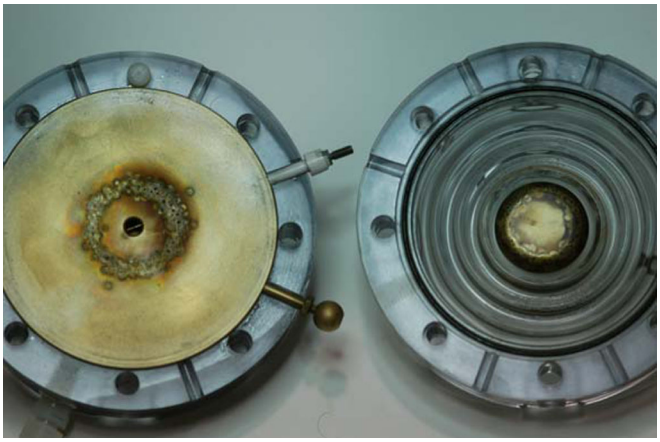

FIG. 10. (Color) L3 Communications, Pulse Sciences gas switch rated for ±100 kV. The brass midplane with its central UV-preillumination gap is shown on the left and the cathode electrode is shown on the right.

III. RESULTS

The results section is divided into several parts. First, we present the self-breakdown curves of our four air-insulated switches. Second, we present waveforms of the brick with each of the four switches when discharged into a matched load and into a short circuit. We will discuss how these waveforms are affected by changes in switch inductances. Third, we look at the results of lifetime tests of the switches. Fourth, we look at resistance of the switch both at matched load and at short-circuit conditions. Fifth, we use optical data to look at the order in which the switch segments break down and the number of breakdown arcs in each gap. Sixth, we discuss problems with the trigger system and possible improvements.

A. Self-breakdown voltages

Figures 11 and 12 show self-breakdown plots of our switches as a function of dry air pressure. Note that in Fig. 11, the self-breakdown curve of the HCEI switch has

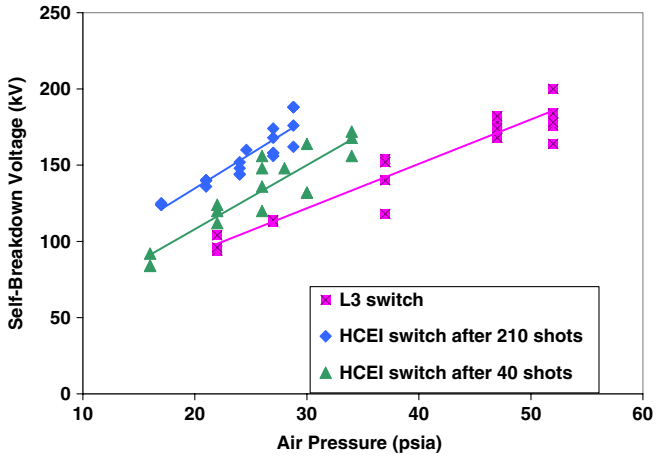

FIG. 11. (Color) Self-breakdown voltages of the Russian and L3 switch as a function of dry air pressure.

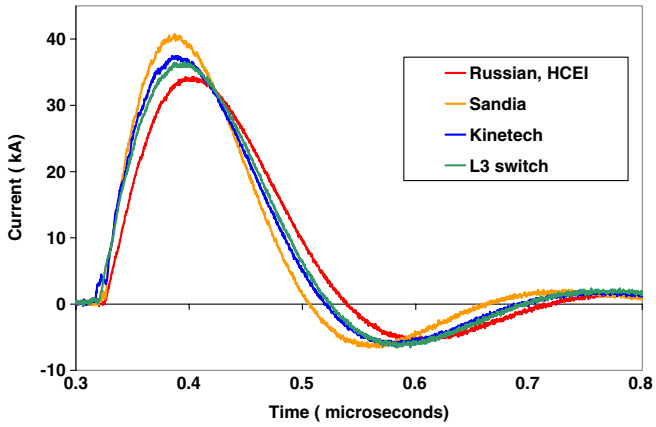

FIG. 13. (Color) Current traces with four different switches in our brick. The 40 nF capacitors were charged to ±100 kV and discharged into a matched load.

shifted upwards after 210 shots as the switch conditions. We were only able to extend our self-break curves to 200 kV since we had + and −100 kV power supplies. This meant that to operate the switches at 200 kV total charge, at ∼70% of the self-break voltage, we had to extrapolate past the high-voltage end of our self-break curves to find an operating point. This extrapolation is shown for the Sandia switch in Fig. 12.

B. Peak currents and switch inductances

Figure 13 shows current waveforms through our brick with each of the four LTD switches we tested. In all cases, the 38 nF capacitors were charged to ±100 kV. The flowing resistive load was adjusted so that the system was always near matched load conditions (∼ 16% current reversal). The peak currents range from ∼34 kA with the HCEI switch to 40 kA with the Sandia-designed switch. The ∼20% increase in peak current seen between the HCEI switch and the Sandia switch is due to the decreased overall circuit inductance when the Sandia switch is substituted for the HCEI switch. These results are summarized in Table II along with command jitter and lifetime measurements that will be discussed later.

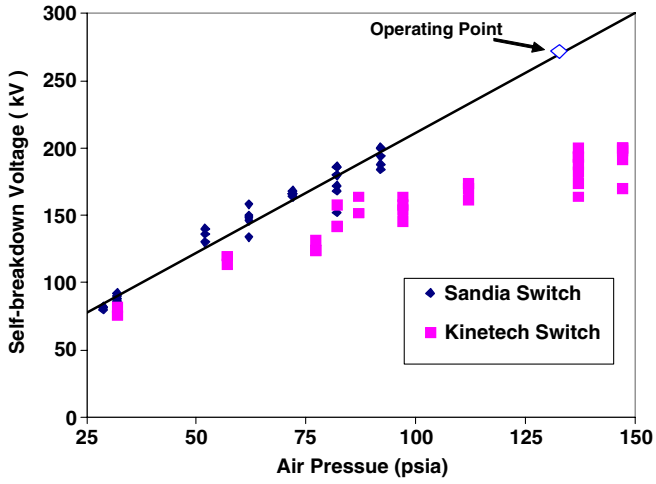

FIG. 12. (Color) Self-breakdown voltages of the Sandia and Kinetech switches as a function of dry air pressure. We extrapolated a fit through each switch's self-break curve to allow us to determine a 200 kV operating point that would have the switch at ∼70% of its self-breakdown voltage. The extrapolated fit and 200 kV, 72% SBV operating point are shown for the Sandia switch.

It is useful to compare these peak currents to the levels produced in the bricks in Sandia's LTD-II cavity [18]. LTD-II has 20 bricks feeding a common resistive load, with each brick having two 40 nF capacitors and one HCEI switch, to deliver a peak current of ∼480 kA (or 24 kA per brick) to a matched load. The differences in peak currents per brick observed on LTD-II and the tests in our brick should be a function of three parameters: (1) differences in the switch inductances; (2) use of single-ended capacitors [24] in LTD-II versus "double-ended" capacitors [20] in our brick and; (3) eddy current losses in the magnetic toroids in LTD-II.

In order to determine the effect of the capacitor type on the peak currents, we performed experiments to directly compare peak currents in a brick with the HCEI switch and

TABLE II. Gas switch matched load operating parameters at ±100 kV charge voltage on 38 nF capacitors.

Switches	HCEI	Sandia	Kinetech	L3
Peak current	33.4 kA	40 kA	37 kA	36 kA
T-rise 10–90	47 ns	40	45	47
T-rise 0–100	76	65	70	74
Delay (ns)	42	41	43	62
1-σ jitter	1.8 ns	5.7 ns	3.3	1.2
% self-break volts	67%	72%	68%	81%
Lifetime	2000	900	>2000	1500

single-ended capacitors to a brick with the HCEI switch and *double-ended capacitors*. We expect higher peak currents with double-ended capacitors because the double-ended capacitors allow us to move the switch closer to the capacitors, which should lower the overall circuit inductance. In our experiments, the peak currents in the brick with double-ended capacitors were about 10% higher than in the brick with single-ended capacitors, confirming our expectations. See Figs. 2 and 3 for a comparison of these two capacitor types.

The currents we measured in our brick with single-ended capacitors and the HCEI switch were still about 27% higher than the currents per brick seen in LTD-II. We would initially expect most of this 27% difference to be due to eddy current losses in the magnetic toroids in LTD-II. However, measurements at HCEI suggest that the current losses in the LTD-II toroids are only about 12% [25]. This leaves about an 18% discrepancy in peak current between our tests and LTD-II results that we do not understand at this time.

Figure 14 shows short-circuit current waveforms for four different switches when the 38 nF-capacitors in our brick were charged to ±60 kV. Again, the brick with the HCEI switch has the longest ringing period of ~370 ns and the brick with the Sandia-designed switch has the shortest period of 330 ns. These ringing frequencies allow us to determine the overall system inductance and hence switch inductance. The decay rate of the signals in Fig. 14 also allows us to estimate the resistance in the system during the discharge process. Our values for these parameters are listed in Table III. We used the ringing periods without correcting for resistive damping in calculating the system inductance since the damping changed the ringing period by less than 1%. To obtain the switch inductance, we subtracted the inductance of the two capacitors (32 nH), the inductance of our flowing resistive load with shorting straps across it ends (~ 24 nH), and the inductance caused by the 1.2-cm wide spacing between the two capacitors (~ 15 nH), from the overall system inductance. Note that our switch inductances include both the inductance of the arc channel in the switch and the loop inductance of the switch and its connections to the capacitors.

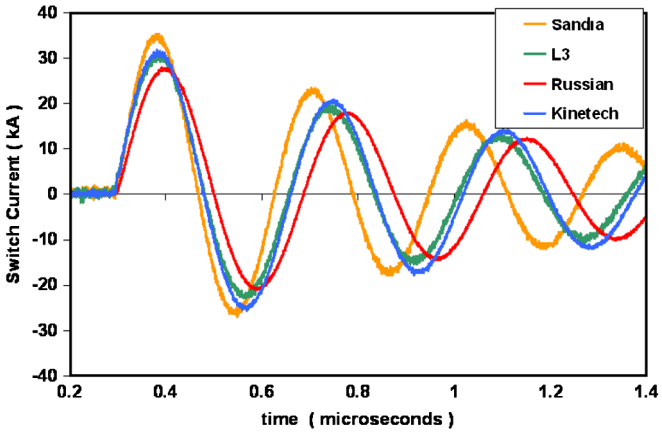

FIG. 14. (Color) Short-circuit current waveforms for our brick with 38 nF capacitors for the four switches we tested. The capacitors were charged to ±60 kV for these tests.

TABLE III. Gas switch short-circuit parameters for ±60-kV charge voltages on 38 nF capacitors obtained from data shown in Fig. 14.

Switch	Ringing period (ns)	System inductance (nH)	Switch inductance (nH)	Impedance after 1st quarter cycle (Ohms)
HCEI	373 ns	185 nH	115 nH	0.37
Sandia	320 ns	136 nH	66 nH	0.32
Kinetech	358 ns	171 nH	100 nH	0.36
L3	352 ns	164 nH	93 nH	0.37

The Sandia-designed switch has only about 66-nH inductance, compared to 93–115 nH inductances for the other switches. This results in a higher peak current (40 kA) and a shorter rise time (40 ns from 10% to 90%) for the Sandia switch.

As a consistency check, we modeled the resistor-inductor-capacitor (RLC) circuit that produced the decaying exponential waveform for the Sandia switch data shown in Fig. 14. After setting the capacitance equal to 19 nF (two each 38 nF capacitors in series) the fit yielded a system inductance of 137 nH and a 0.34 Ohm circuit impedance. These values are in excellent agreement with the system inductance and resistance listed for the Sandia switch in Table III.

C. Delay, jitter, and lifetime measurements

Table II also lists the results of our delay, jitter, and lifetime measurements for these four switches. We typically took two shots a minute in the lifetime tests, purging the air in the switch between each shot. For the Sandia, Kinetech, and L3 switches, these results were obtained using a trigger pulse at the switch with an 80 kV peak voltage and a 10–90 rise time of 26 ns. For the Russian switch the trigger voltage was 120 kV with a rise time of 12 ns. The differences in these trigger voltages measured *at the switch* are related to coupling issues between the trigger generator and the switch and are discussed below.

We will now discuss the delay, jitter, and lifetime measurements for each of the four switches in detail. All of these measurements were made with two 40-nF capacitors in the brick that were charged to ±100 kV.

The HCEI switch lifetime data is shown in Fig. 15. We took more than 100 shots on this switch at voltages below 100 kV before beginning this run as the HCEI switch is known to have a ‘‘conditioning period’’ before achieving its rated jitter. This switch still had high 1-σ jitter, over 100 ns for the first 50 shots. After that, the switch jitter was

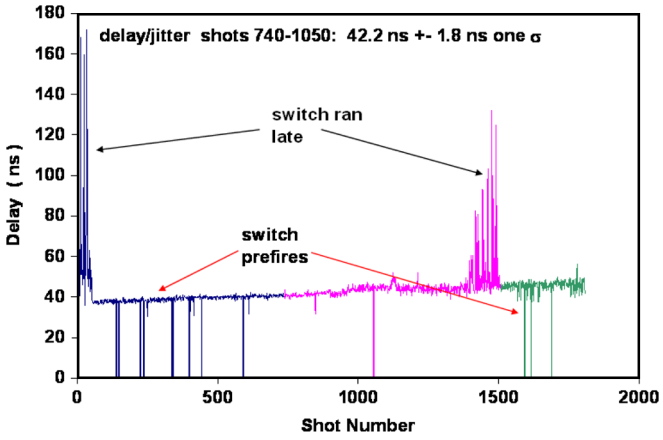

FIG. 15. (Color) Lifetime test results for the Russian switch at a ±100 kV charge voltage. The switch was operating at 67% of the switch's self-breakdown voltage. The data was taken on three successive days as indicated by the color coding of the data.

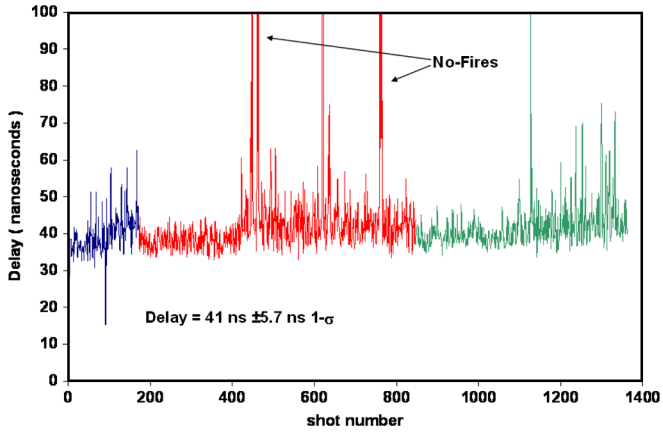

FIG. 16. (Color) Lifetime test results for the Sandia switch. This switch was operating at 72% of its self-breakdown voltage. The data was taken on three successive days as indicated by the color coding.

less than 2 ns, but the switch had 12 prefires in the next 1600 shots. The switch also had another period of high jitter (over 10 ns), between shots 1400 and 1500. After shot 1800 we removed the switch from the test apparatus and discovered that one of the five toroidal electrodes had come loose and fallen onto the electrode below it during the 1800 shot run. We also observed a number of surface tracks on the interior of the polycarbonate insulator.

We would expect low jitter from this switch since the trigger pulse only has to break down 1/6 of the total gap voltage to start the triggering process. The prefires are surprising as we were operating at 67% of the nominal self-break voltage. Other researchers have achieved low jitter operation with no prefires at ±100 kV charge since our experiments by operating this switch at 62–65 psia [26]. The loosening of the toroidal electrode is also surprising. The toroidal electrodes are screwed onto brass spheres that lock the electrodes into place by fitting into grooves cut in the inside diameter of the switch insulator. If the brass spheres come loose, the electrode can drop onto its neighbor. In other tests, however, this type of problem has only been seen after ~10, 000 shots on the switch [26]. Our experiments did have higher peak currents than previous experiments, but had the same overall energy transfer per shot.

The Sandia switch lifetime results are shown in Fig. 16. This figure shows data taken on three successive days. This switch did not show a significant conditioning period and had an average delay of 42 ns and a 1-σ jitter of ±5.7 ns. The switch's relatively large jitter may be due to several factors: First, we had an 80 kV trigger pulse for these experiments. Second, this switch has only two gaps and hence the trigger pulse must break down ~50% of the switch voltage instead of ~16% of the switch voltage as was the case with HCEI switch. Third, the switch had uniform field grading on the electrode surfaces, which allowed the switch to hold off voltage at lower gas pressures, but also made it more difficult to trigger (Fig. 7). The switch's jitter appeared to deteriorate late in each day, which may be due to thermal effects. This switch failed to trigger several times during the ~1350 shot run. More seriously, on three occasions, the switch suffered external arcs through the oil between the field-grading "doughnut" on the midplane and the switch end plates. Each of these arcs destroyed one or more of the plastic rods holding the switch together and forced a rebuild of the switch.

The Kinetech switch lifetime results are shown in Fig. 17. These 2000 shots were taken over four successive days. The switch had an average delay of 41 ns and a 1-σ jitter of ±3.3 ns. Two prefires occurred on the first day. The average delay, which started at 40 ns, drifted about 5 ns later over the course of the 2000 shot run. After the run, the switch was taken apart and examined and showed no signs that it was nearing the end of its useful life. This

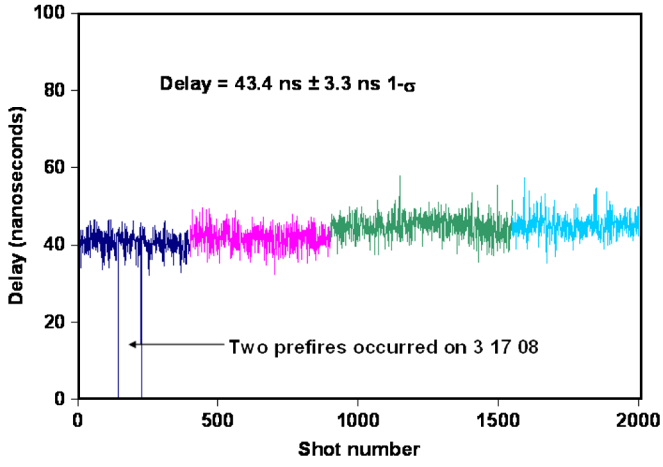

FIG. 17. (Color) Lifetime testing results for the Kinetech switch. This switch was operating at 68% of its self-breakdown voltage. Data was taken on four successive days.

switch's jitter may be lower than the Sandia switch because the radiused ends of the 0.63-cm diameter trigger pins had much higher field enhancements than the midplane on the Sandia switch during the triggering process.

The L3 Pulse Sciences switch lifetime data is shown in Fig. 18. These 1678 shots were taken over four successive days. Most of these shots were taken at 81% of the switch's self-breakdown voltage. The lifetime tests on the other switches were taken at 67%–72% of the switch self-break voltages. This switch had two early prefires and then only one no fire in the first 933 shots. The 1-σ jitter during this period was an impressive ± 1.2 ns and the average delay was 45 ns. This low jitter is probably related to the relatively high percent of self-break voltage during these experiments and the fact that this switch had a UV-preillumination pin in the midplane that flooded the switch with UV light when the switch was triggered. At the end of the second day, our system had an arc in the oil that was not related to problems with the switch. The arc, however, tracked a gas line to the switch, filling the switch with oil, and forcing a switch rebuild. On the third day (after the rebuild), the switch began prefiring. We raised the pressure to 70 psig on the next day in an attempt to stop the prefires. Because we increased the pressure, the switch was now operating at approximately 70% of its self-break voltage. The pressure increase stopped the prefires, but it also increased the delay to 62 ns and the 1-σ jitter to ± 6 ns. At the end of the 1679 shot run, we disassembled the switch and found that the cast epoxy insulator separating the UV-preillumination pin from the electrode was shattered. We suspect this damage occurred during the oil arc at the end of the second day. Hence, the UV-preillumination pin may not have been working properly on the final two days of the run. L3 is replacing these relatively brittle cast epoxy insulators with machined plastic insulators that may solve this problem.

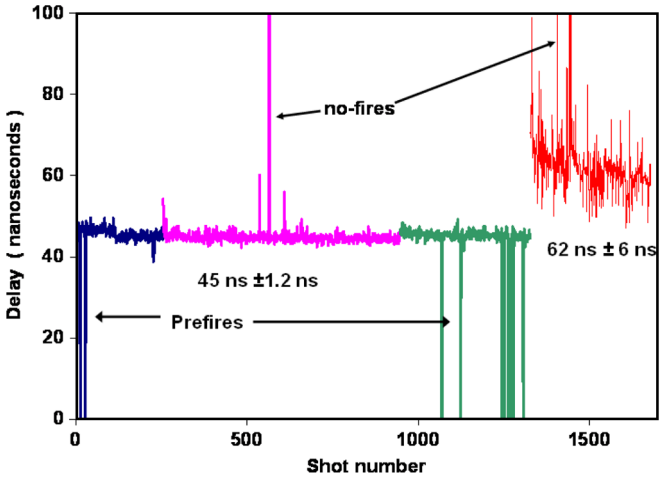

FIG. 18. (Color) Lifetime test results for the L3 Pulse Sciences switch. During the first 3 days (blue, purple, and green traces) this switch was operating at 81% of its self-breakdown voltage. During the last day (red trace) it was operating at 70% of its self-breakdown voltage.

D. Triggering at low voltages

Sandia has some switch applications that require gas switches to be DC charged to ± 100 kV and then triggered at a later time when the voltage across the switch has been reduced to ± 60 kV or less [27,28]. To support these applications, we attempted to trigger our switches when they were at the gas pressure required for ± 100 kV shots, but with reduced voltages across the switches. When the pressures in the switches were set at the levels required for ± 100 kV operation (listed in Table I), the Kinetech, Sandia, and L3 switches would not trigger below charge voltages of ± 75 kV. The Russian switch triggered at least down to ± 70 kV. Other experiments at Sandia suggest that, under these conditions, the Russian switch may trigger at charge voltages below ± 60 kV [29].

E. Impedance and inductance measurements

We measured system impedance in two ways. First, we measured the impedance of the entire brick during the short-circuit shots by simply measuring the exponential decay rate of the envelope of the current oscillations. We did not use data from the first half cycle of current since we suspected the resistance of the switches was changing during that time. This system impedance data from the decay rate of the current envelope is listed in Table III shown above. Table III shows switch impedances on the order of 0.3–0.4 Ohms under short-circuit conditions for all four switches.

Second, we attempted to determine the impedance of the switch itself by measuring the voltage directly across the switch during the discharges. These switch voltage measurements were made with capacitive voltage monitors (V dots) looking at the switch top and bottom end plates as shown in Fig. 4. We could make these switch resistance measurements both under matched load and short-circuit conditions. The time-dependent voltage V_s across the switch during the breakdown process will have both resistive and inductive components:

$$V_s = IR + LdI/dt, \tag{1}$$

where I is the switch current, R is the resistance of the discharge arcs, L is the inductance of the discharge arcs, and dI/dt is the rate of change of current through the switch.

The switch resistance is then simply

$$R = (V_s - LdI/dt)/I. \tag{2}$$

We can estimate the resistance of the discharge arcs either by looking at the switch voltage at the current maxima and minima when LdI/dt is zero, or by estimating L and then subtracting LdI/dt from the voltage across the

switch. Since we expect the arc resistance to be relatively constant after the first half cycle, the "best" value of L will be the one that produces a constant R value at late times. This final technique of measuring resistance has the added benefit of producing an estimate of the inductance of the discharge arcs.

The inductance we estimate using the V dots and LdI/dt corrections is actually the arc inductance plus any self-inductance in the switch hardware between the top and bottom plates of the switch. For the Sandia, HCEI, and L3 switches, this "hardware inductance" is negligible relative to the arc inductance. For the Kinetech switch with its narrow electrode stalks, we estimate [30] that this "hardware inductance" is between 10 and 30 nH. Further, there is some doubt whether the Kinetech switch electrode actually contacted the switch end plate. If these parts did not make contact, then all of the switch current would have been forced to flow through the small 6–32 screw holding these two parts together, further adding to the "hardware inductance" of this switch. Because of these problems, our arc inductance measurements for the Kinetech switch give us only an upper limit to the true arc inductance.

Figure 19 shows plots of the voltages on top and bottom of the Sandia switch along with a current trace under short-circuit conditions. Figure 19 also shows estimates of switch resistance at the times of peak current (when $dI/dt = 0$). During the first half cycle, Fig. 19 shows a switch impedance of ~0.55 Ohms. After the first half cycle, the switch impedance is ~0.15–0.3 Ohms.

Figure 20 shows switch resistance versus time using the LdI/dt corrections and three different "guesses" for the inductance L of the discharge arcs in the Sandia switch.

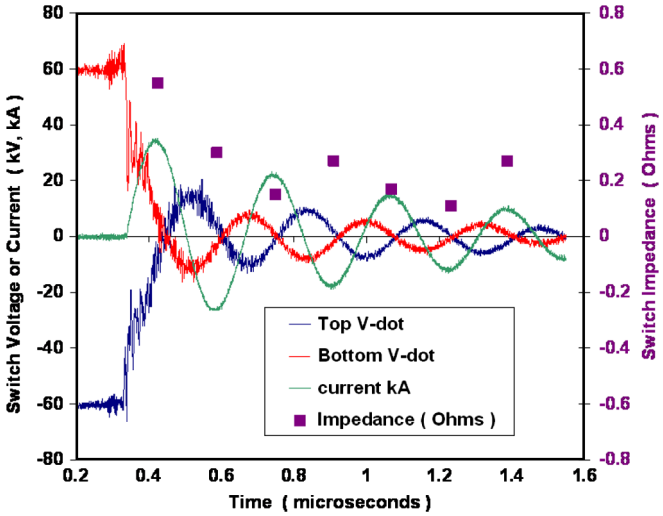

FIG. 19. (Color) Voltage on top and bottom of the Sandia switch and switch current for a ±60 kV shot into a short circuit. We could directly calculate switch impedances at each of the peaks of the current waveform from the voltage and current measurements. These values of impedance are shown in purple and their values are listed on the right-hand scale.

The top plot with $L = 0$ shows the impedance going negative on each current half cycle, which is clearly nonphysical. After the first half cycle, the bottom plot with $L = 50$ nH shows impedance rising during each half cycle and then resetting to a lower value at the start of the next half cycle. Again, this seems highly unlikely. The middle plot with $L = 30$ nH shows relatively flat impedances after the first half cycle, in line with switch impedance models that predict that the impedance will approach a constant value at late times. Thus, we assume that the discharge

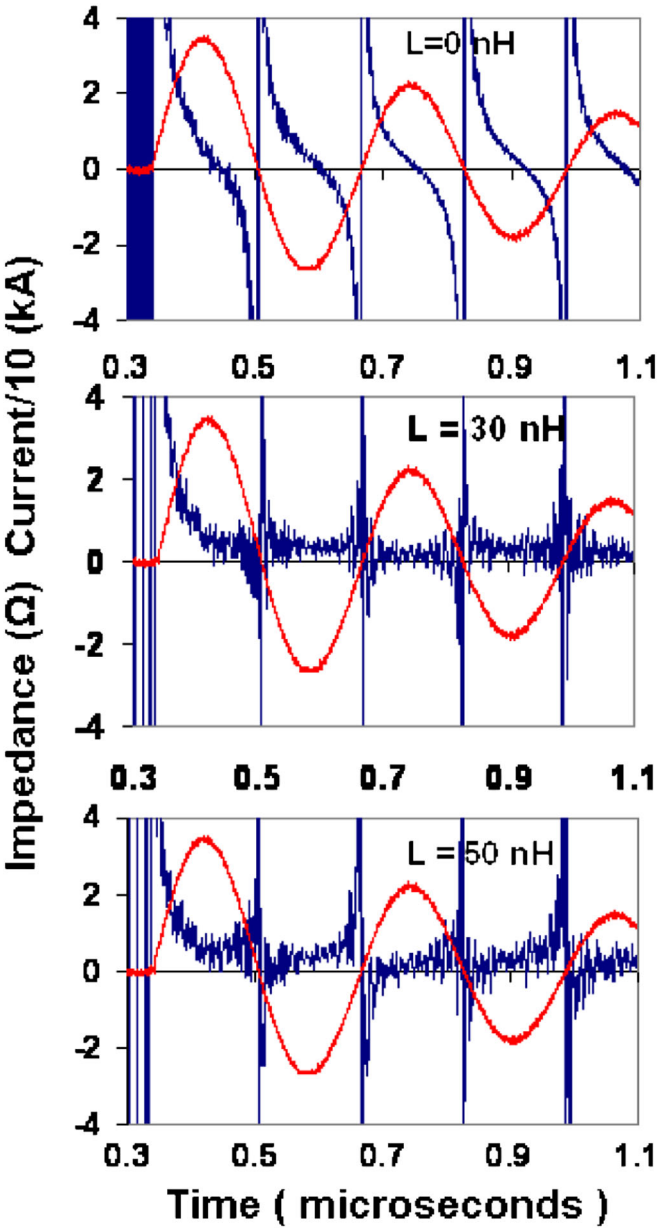

FIG. 20. (Color) Plots of brick current and Sandia switch impedance when the brick with the Sandia switch was charged to ±60 kV and then discharged into a short-circuit load. Three different assumptions for switch inductance (L) are shown. Only the middle plot, with $L = 30$ nH gives physically reasonable results.

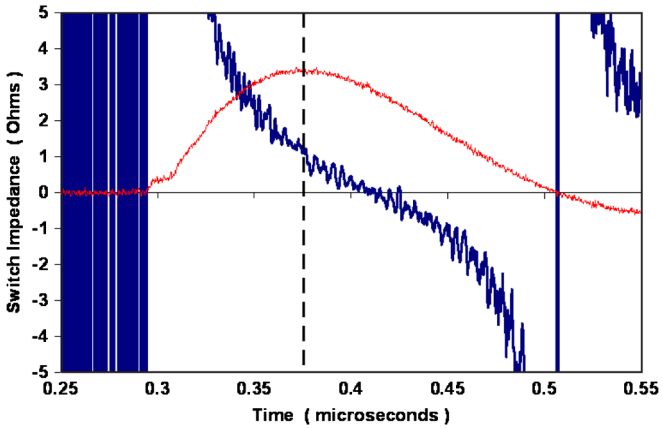

FIG. 21. (Color) Graph of impedance versus time for the Kinetech switch when the brick was charged to ±100 kV and discharged into a matched load. Since we have not made any inductive corrections, the graph is only accurate at peak current (indicated by a dashed vertical line), where the graph shows an impedance value of 1.2 Ohms.

channel impedance is approximately 30 nH or 13 nH/cm. This 13 nH/cm value is in reasonable agreement with 13–17 nH/cm discharge channel inductance estimates made by others [31]. Similar analysis of data from the Kinetech switch produced much higher arc inductance estimates. The total measured inductance between the end plates of the Kinetech switch was 55 nH. As stated above, much of this inductance was probably due to constrictions in the switch hardware rather than in the arcs themselves.

The impedance values obtained from the V-dot monitors are for the switch itself and do not include the contribution to the system impedance caused by the inductance of the current loop formed by the switch and its connections to the capacitors. We would therefore expect the V-dot impedances to be slightly lower than the overall impedances measured from the decay of the current envelope listed in Table III. Hence, we consider the values of impedance from the V dots and the decay of the current envelope to be in reasonable agreement.

When the brick is discharged into a matched load, the V-dot monitors give very different results. Figure 21 shows a plot of current through the Kinetech switch discharged into a matched load after the capacitors were charged to ±100 kV. Since we made no inductive corrections to this data, it is only accurate at peak current—the location of the dashed vertical line. At this time, the switch impedance is ~1.2 Ohms. All four switches showed matched load impedances between 0.8 and 1.2 Ohms at peak current. In previous experiments, the HCEI switch was attached to *20 nF capacitors* charged to ±200 kV and discharged into a critically damped load. Under these circumstances, we measured a switch impedance of 3.7 Ohms at peak current. These results suggest that the impedance of the switch itself is strongly affected by the balance of the circuit.

F. Optical measurements

We used two optical diagnostics in these tests. The first was a fast framing camera with the capability of taking eight frames with a minimum frame time of 5 ns. The second diagnostic consisted of an array of optical fibers with each fiber apertured to accept light from only one of the electrode gaps in these multigap switches. The optical fibers were led to an array of photomultiplier tubes and allowed us to observe turn-on delays in the light from the various switch gaps.

We tested the Russian switch with bricks using both 20 nF capacitors and 40 nF capacitors. Figure 22 shows a timing plot of a shot of the turn-on of the Russian switch attached to 20 nF capacitors and discharged into a critically damped load. The figure shows switch current in kA along with the trigger signal at the switch and (negative) light signals from photomultipliers looking at the upper five of the six gaps in the switch. The third gap is the triggered gap and emits light about 5 ns before the two gaps above it. There is about a ~10-ns delay after the top three gaps break down before the bottom gaps break down, the main current pulse begins and the light becomes very bright. The times of seven pictures taken by the framing camera are indicated in the top half of Fig. 22 and the pictures themselves are shown in Fig. 23. First light occurs in the trigger gap in the 2nd frame (labeled 10 ns). The gap above the trigger gap breaks down in the third frame and all but the bottom gap (6) have broken down by the end of the 4th frame. Small light "dots" above and below some of the discharges are light that has been refracted through curved areas on the insulator surface. Gaps 1 and 6 are only visible through light refracted this way. The toroidal electrodes in this switch are designed to spread current through multiple arc channels in each gap in order to lower the overall switch inductance. Given that we see only one arc in two

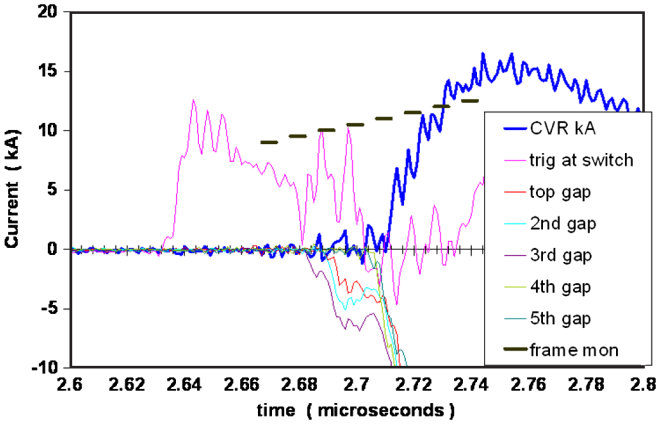

FIG. 22. (Color) Graph of trigger voltage, switch current, and negative light signals on shot with the Russian switch discharging two each 20 nF capacitors. The times of the 5-ns-wide framing camera images in Fig. 21 are also listed. The trigger voltages and light signals are in arbitrary units.

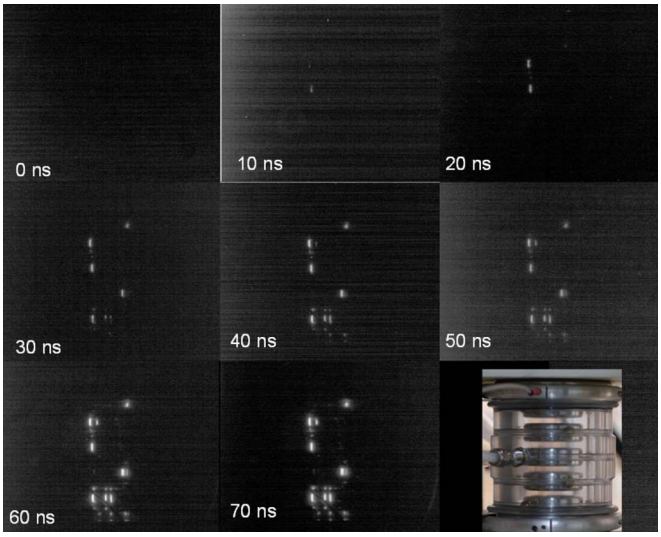

FIG. 23. (Color) Framing camera images of light emitted by the HCEI switch during the breakdown process. The frames were 5-ns wide and started at 10-ns intervals. Note that the light starts in the triggered gap, migrates to the top of the switch, and then to the bottom of the switch. Also note that three of the gaps only have one breakdown arc.

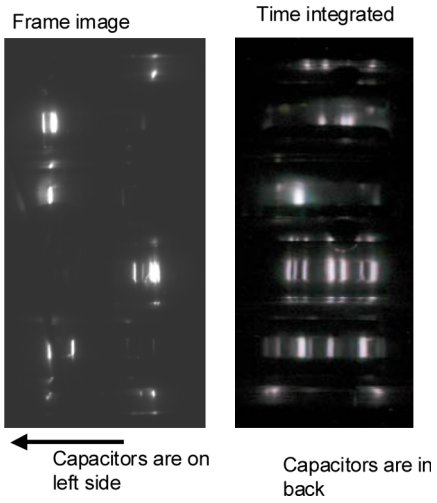

FIG. 24. Images of the Russian switch breakdown taken 90 degrees apart from each other. The left image is a 10 ns frame picture and the right image is a time-integrated picture. While there are multiple arcs in most gaps, the arcs tend to cluster in small areas of the electrodes, which limits the impact of the multiple arcs on the switch inductance.

of the switch gaps and only two closely spaced arcs in two more gaps, which was typical of the 20 nF data, the multichanneling is unlikely to significantly lower the switch inductance in circuits using 20-nF capacitors.

Figure 24 compares two views of the arcs in the Russian switch in a brick with 40 nF capacitors charged to ± 100 kV and discharged into a matched load. This figure shows two views of the same shot: (1) a 10-ns wide framing camera picture taken during the rise of the current and (2) a time-integrated picture which was taken at a 90° angle to the framing camera view. The time-integrated picture shows significant multichanneling in the majority of the gaps, but the frame picture at 90 degrees shows that most of the arcs in each gap are clustered closely together. Further, the arcs in one gap do not line up with the arcs in its neighbors, which will also tend to increase the switch inductance. Again, the bottom half of the switch, which breaks down last and probably sees a much higher dV/dt than the top half of the switch, has more multichanneling than the top gaps. This type of switch has also been used in Marx generators with much larger capacitors. In these Marx-type applications, multichanneling and the consequent lowering of switch inductance may be much more important.

We also recorded framing camera data with a modified version of the Kinetech LLC switch. The modified switch we used for these tests had a special inner housing of polished acrylic. The outer insulator had a 1.27-cm diameter hole in it to allow us to view the discharge region through the clear acrylic. Figure 25 shows timing information for a ± 100 kV shot of the Kinetech switch, including times of the framing camera pictures along with the trigger voltages and the switch current. The framing camera pictures themselves are shown in Fig. 26. We used two 40-nF capacitors in these tests and the brick was discharged into a matched load. The switch pressure was 242 psia. The camera frames are 10 ns long, with no dead time between frames. The triggered (upper) gap in the switch shows a diffuse glow while the trigger voltage is rising in the "10 ns" frame. This glow constricts to an arc and the

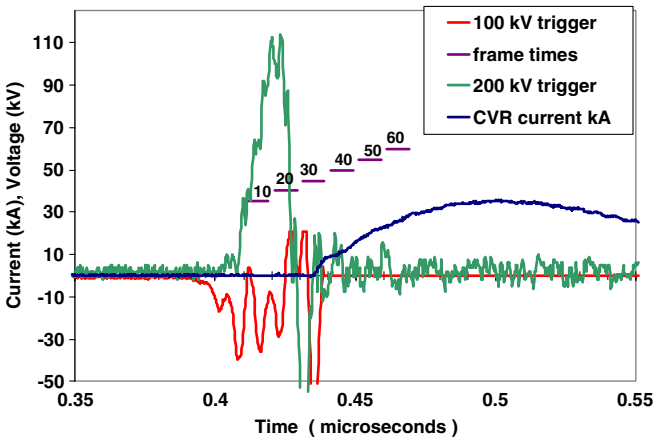

FIG. 25. (Color) Timing plot for a Kinetech switch shot with the 40 nF capacitors charged to ± 100 kV. For this data we used the two-stage trigger system discussed in Sec. III G in which the pulse from our trigger generator triggered a switch with 100 kV total voltage across it. The output from the 100 kV switch was used to trigger the ± 100 kV Kinetech switch. Both the initial trigger for the 100 kV and the final trigger to the ± 100 kV (200 kV total voltage) switch are shown. The plot also shows the current trace and the times when the 10-ns-wide framing camera pictures were taken.

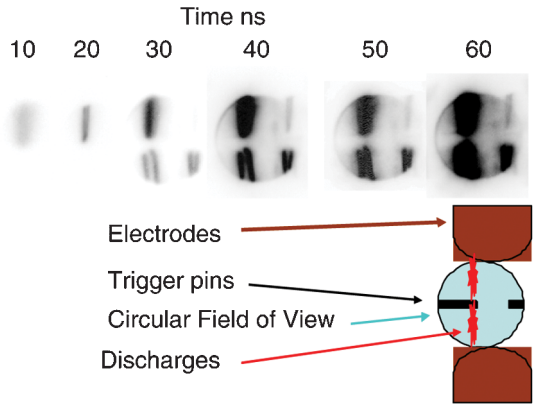

FIG. 26. (Color) Framing camera images of the breakdown of the Kinetech switch after the 40 nF capacitors are charged to ±100 kV. Current must flow outside the switch to drive three of the four breakdown arcs seen in the bottom half of the picture.

trigger voltage collapses in the "20 ns" frame. In the "30 ns" frame, arcs are growing from all four trigger pins to the bottom electrode and the main current pulse through the switch has begun. In the remaining frames the arcs get brighter, with the two arcs connecting the top and bottom electrodes through the trigger pin on the left of the picture appearing to dominate.

It is interesting that only one arc appeared in the top of the switch but all four trigger pins broke town to the bottom electrode. This means that, after the top gap broke down to one trigger pin, current traveled ~20 cm out of the switch to the point where the trigger cables for the four trigger pins join, then traveled back into the switch to break down the lower gaps. This odd current path may have been assisted by UV illumination inside the switch. The initial arc between the top electrode and the trigger pin flooded most of the inside of the switch with UV light, which would assist the breakdown of three of the lower gaps. The trigger pin connected to the first arc, however, would block UV light from reaching the gap immediately below itself. Thus, the three "UV-illuminated" lower gaps not immediately connected to the upper arc would have a lower breakdown strength, favoring the relatively high-inductance current path out and back the trigger cables. The lower-inductance path, straight from the upper electrode through one pin and to the lower electrode appears to predominate by the time the current has reached half its peak value. We could probably suppress this unusual current path by adding ballast resistors to each of the trigger pin connectors, but it is not clear that this would improve the switch performance.

G. Trigger system issues

During these experiments, it became clear that a gas switch and its trigger system must be considered together as one coupled system. The two cannot be considered in isolation.

For most of our experiments, our trigger generator was a two-stage Marx with an erected capacitance of ~3 nF and an erected voltage of ~75 kV into a matched 50 Ohm load [32]. Our switch trigger electrodes, however, look like an open circuit before the switch breaks down and this trigger generator typically produces a 120 kV pulse into an open circuit with a rise time of about 8 ns. On the advice of the trigger generator manufacturer, we inserted a 360 Ohm resistor between the trigger generator output and our switches to protect the trigger generator from voltage oscillations that might occur on the trigger plane when the switch fires. This setup is shown in Fig. 28.

We expected that there would be about ~10 pF of capacitance between our trigger planes or pins and the top and bottom switch electrodes. This ~10 pF of capacitance and the 360 Ohm trigger resistor would form an RC integrator circuit that would limit our trigger rise times to values longer than ~3.6 ns. Since our trigger rise times were ~8 ns, this limitation did not appear to be a problem. Late in our experiments, we began monitoring the trigger voltage at the switch with the 5.1 k-Ohm and 30 Ohm resistive divider shown in Fig. 28. This monitor indicated that the trigger pulse *at the switch* only reached 80 kV and had a rise time greater than 20 ns as shown in Fig. 27. Replacing the 360-Ohm series resistor with a 50-Ohm resistor restored the full 120-kV, 8-ns rise time trigger pulse at the switch. The difference in the wave shapes with the 360 and 50 Ohm resistors suggests that our "RC integrator" circuit in the trigger system actually had a $1/e$ rise time of ~28 ns, not 3.6 ns. This indicated that the total capacitance of our midplane, including known and stray capacitances, is about 70–80 pF. Since the 360 Ohm resistor had been used to protect the trigger generator, we relocated the trigger monitor upstream (on the trigger generator side) of the 50 Ohm resistor for one shot to see

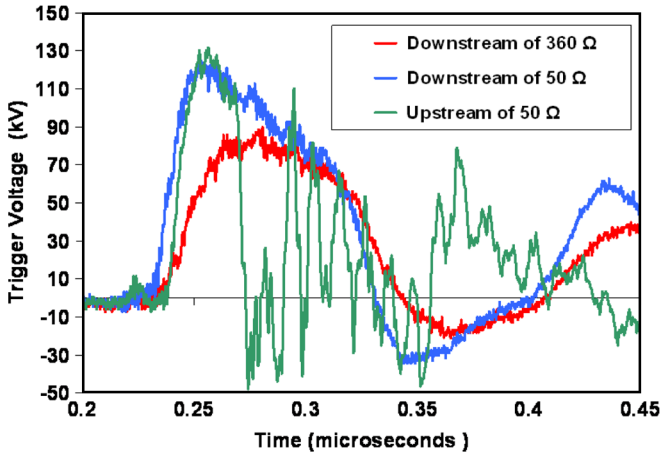

FIG. 27. (Color) Trigger pulses measured at the L3 gas switch and upstream of the 360 Ohm protection resistor for the trigger generator. Unexpectedly large stray capacitances were degrading the rise time of the trigger pulse at the switch when the 360 Ohm resistor was in place.

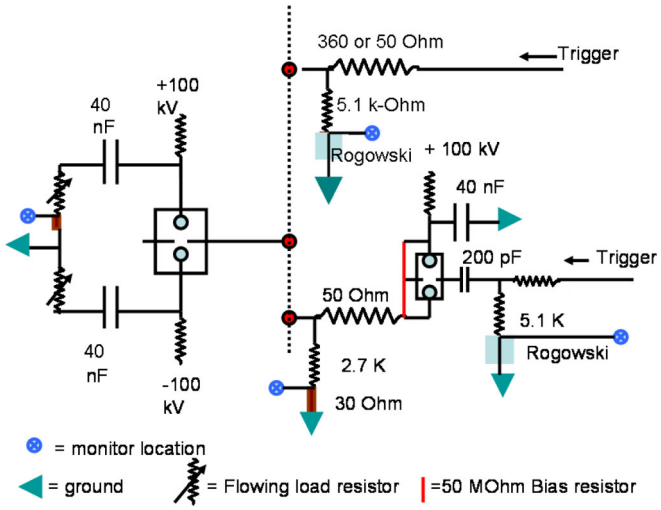

FIG. 28. (Color) Schematic of the two trigger circuits used in these experiments. The LTD brick is on the left. The original trigger system consisting of the L3 trigger generator with a 360 or 50 Ohm series resistor is on the upper right. The final trigger system that has an extra stage of power amplification is at the lower right.

if our system was inducing unacceptable voltages on the trigger generator when our switch fired. Since the voltages upstream of the 50 Ohm resistor were no larger than the voltages normally in the trigger generator, we concluded that using the 50 Ohm series resistor would not cause problems. Our jitter and lifetime measurements for the Kinetech, Sandia, and L3 switches were made using the 360 Ohm trigger resistor. The jitter and lifetime measurements for the Russian switch were made using the 50 Ohm resistor, which would tend to give lower jitter measurements for the Russian switch.

Our concerns about our trigger system led us to develop the two-stage trigger system also shown in Fig. 28. In this system, our original trigger generator triggers a 100-kV switch. This 100-kV switch then discharges a 40 nF capacitor into the trigger electrode of our ± 100 kV switches. This system was used when we were taking framing pictures of the Kinetic switch, and the trigger voltages to the 100 kV and 200 kV switches are shown in Fig. 24. This two-stage system more closely resembles the trigger systems used in existing LTD cavities.

IV. DISCUSSION

A. Switch inductances

In Sec. III, we presented approximate switch inductances derived from the discharge current waveforms of our brick. There were some surprises in these results, particularly the relatively high inductance of the small Kinetech switch. It is useful, therefore, to consider what aspects of the switch designs led to high or low inductance and to make first order estimates of switch inductance based on the switch geometries. In estimating the inductances, it is important to note that the circuits containing these switches are not in a coaxial configuration.

Several factors contribute to the overall inductance added to the circuit by the switch. First, there is a current loop running from the top capacitor contacts, through the switch and back to the bottom capacitor contacts (see Fig. 3). The area of this current loop or ''single-turn solenoid'' is a major contributor to the inductance added by the switch. The inductance contributed by this loop will vary linearly with the loop area. Second, constrictions in the switch geometry itself will add inductance. Simply put, a large diameter wire will have a lower self-inductance than a small-diameter wire of the same length. Thus, we would expect the large cross-sectional diameter electrodes in the Sandia switch to have lower self-inductances than the much smaller cross-sectional diameter electrodes of the Kinetech switch. Third, the small-diameter discharge arcs in the switch will have an important impact on the overall system inductance. Experimental results with the Sandia switch suggest arc inductances of 13 nH/cm of arc length in agreement with measurements by others [31]. Experimental results with the Kinetech switch are complicated by the relatively high inductance on the small-diameter electrode stalks and the possibility that all of the switch current may have had to flow through the small 6–32 screws connecting the electrodes to the switch end caps. Our data shows ~55 nH of inductance between the top and bottom of the Kinetech switch, but we are unable to determine how much of this inductance is due to the arcs themselves.

We have not found any simple analytical expressions that capture all three of the factors listed above. We have gotten the best results by approximating the switch circuits as short solenoids and then adding the expected arc inductance.

The inductance of a short solenoid was originally calculated by Nagaoka [33] and more recently presented by Grover [34]:

$$L = 0.004\pi^2 a^2 N^2 K/b, \tag{3}$$

where L is the inductance in Micro-Henrys, a is the solenoid radius in cm, N is the number of turns (one in our case), b is the length of the solenoid in cm, and K is a factor that takes into account the effect of the ends. K is a slowly varying factor that has values of 0.20, 0.37, 0.52, 0.62, and 0.69 for solenoid length-to-diameter ratios of 0.10, 0.25, 0.50, 0.75, and 1.00, respectively.

In Eq. (3), to first order, the inductance depends linearly on πa^2, the cross-sectional area of the solenoid, and inversely on b, the length of the solenoid. Grover [34] has demonstrated that the solenoid need not be circular for this to be true.

We can easily determine the cross-sectional area of our ''solenoids.'' Determining their length is more difficult.

TABLE IV. Calculated and experimentally measured switch inductances.

Switches	HCEI	Sandia	Kinetech	L3
Solenoid loop area cm^2	115	48.4	45.2	62.9
Average length of solenoid cm	7.33	7.5	4.18	5.3
Area/length cm	15.7	6.4	10.8	11.8
K	0.570	0.679	0.549	0.566
L without arc contribution nH	112	54	74	84
Arc L	40[a]	30[a]	55[c]	38[b]
Total calculated L value nH	152	84	129	122
Experimental L value nH	115	66	100	93

[a]Experimental value measured during this work.
[b]Literature value assuming 15 nH/cm.
[c]Experimental measurement of total inductance between switch end caps—arc inductance will be lower.

The solenoids all have a 7.6-cm length where they attach to the capacitor tabs, but they become much narrower in the switch. In the ''stalks'' connecting the Kinetech switch electrodes to the end caps, the ''solenoid'' is only 0.7 cm wide (Fig. 8). We chose to define an ''average length'' of the solenoid by breaking the solenoid into sections of equal length, weighting the sections by the width of each section and then summing the sections to arrive at an average length. We caution that Nagaoka's formula does not treat solenoids whose length varies as the current flows around the solenoid, so our calculations will only be first order approximations. Note that these solenoid inductances neglect the arc inductances, which will need to be added separately. Table IV presents our calculated cross-sectional areas, average lengths, K values, and first order inductances for the four switches installed in our brick and compares them with the inductances we measured experimentally. For the Sandia, HCEI, and Kinetech switches, we use the arc inductances we measured experimentally. For the L3 switch we used the 15 nH/cm inductance estimate taken from the literature [31].

While the calculated inductance values show the proper trends relative to the experimental measurements, the calculated values are 20%–32% larger than the measured values. The crudeness of our average solenoid length calculations probably contributed to these disagreements. Another source of error comes from the fact that our ''bricks'' are wrapped in a four-sided metal box (see Fig. 1). This will constrict the magnetic field produced by the solenoid and alter the solenoid inductance.

B. Switch performance

None of the switches we tested are ideal. The baseline HCEI switch has a number of advantages. It is robust, it works at relatively low pressure, and it is easy to trigger since the trigger only has to break down one of six gaps. However, its large size makes it relatively high inductance ($\sim$ 115 nH) and as a six-stage gap is complex and hence relatively expensive. It also required extensive conditioning (more than 100 shots) at lower voltages before going to the full $\pm$100 kV charge. In other tests, this switch has performed well for over 10 000 shots. In our lifetime tests, this switch fell apart internally in less than 2000 shots. This failure mode has recently been seen by other experimenters who have added a thread-locking compound to the bolts inside the switch holding the electrodes in place to solve the problem. The arcs we saw on the internal surface of switch housing may have been caused by our using a polished polycarbonate housing instead of the normal Caprilon or nylon housing. Impurities left on the surface by the polishing process may have been more important than the material type as polycarbonate housings were used successfully in the L3 switch.

The Sandia-designed switch has by far the lowest inductance (66 nH) of any switch we tested and is relatively simple and inexpensive. However, the E-fields on the outside of the switch appear to be too high for reliable operation, leading to occasional external arcs in the oil. These arcs appeared to be through the oil, and not along any surface. Since these arcs normally destroyed one or more of the switch rods, modifications are clearly needed to reduce the external fields on this switch.

The Kinetech, LLC switch is very robustly designed, relatively simple, and triggers with less than 5 ns jitter. It had the best operation over the 2000-shot lifetime run of any of the switches we tested. It operates at relatively high pressure $\sim$242 psia which might pose problems in some applications. The switch's inductance is surprisingly high ($\sim$ 100 nH) for a switch this small. It seems likely that the high inductance of this switch is caused by the relatively small-diameter ''stalk'' connecting the electrode to the switch end plate (see Fig. 8). Further, it is possible that the copper-tungsten electrode never actually contacted the aluminum end plate directly and that all the current was forced to flow through the small 6–32 bolt holding the end plate to the electrode. We have designed new electrodes and end caps for this switch that more than double the diameter of the stalk and improve the contact between the electrode and the end plate.

The L3 switch, which is relatively short (7.6-cm tall) and relatively large in diameter (14.6 cm), is a modification of a $\pm$50 kV switch that was designed to nestle between the insulation barriers of single-ended capacitors in small Marx generators. Hence, it is far from the optimal shape for our use. We mounted it in our brick in a low-inductance configuration, with wide current bars connecting directly from the capacitors to the ends of the switch. Under these conditions, the switch added only about 93 nH of inductance to our system. The switch jitter was less than $\pm$2 ns at $\sim$81% of the self-break voltage, but we do not have a good jitter test at $\sim$70% of self-breakdown voltages (SBV). The cast epoxy insulator on the switch's UV illumination pin is too fragile. The manufacturer is replacing

this epoxy with a machined plastic piece that may solve this problem. To examine whether this basic switch design can be pushed to lower inductances, we have asked the manufacturer to design smaller diameter version of this switch.

Our problems with the trigger system illustrate the importance of measuring the trigger voltage at the switch. The unexpectedly large stray capacitances we found were probably due at least in part to the ground plane wrapped around our brick. It seems important therefore, in assessing whether a trigger system is adequate, to have the switch mounted in whatever container it will eventually be used in so that the testing will be done in the presence of all of the stray capacitances that will occur in the final application.

V. SUMMARY

We directly tested four 200-kV air-insulated gas switches against each other for use in future linear-transformer-driver accelerators. The peak currents we observed in our ''single brick'' LTD test bed experiments are 67% higher (40 vs 24 kA) than the current per brick observed on the LTD-II 500-kA cavity for identical charge voltages and brick capacitances. About 20% of this increase was due to improvements in switch design. About 10% of the increase was due to improvements in capacitor design. At least 12% of the increase was due to eddy current losses in the magnetic toroids used in the LTD-II cavity. Our test setup did not have magnetic toroids, which are required in any real LTD cavity. We cannot account for the remaining 18% increase in current at this time. Further work is needed to understand this discrepancy and reduce the losses in the toroids.

Of the three new switches, only one, designed by Kinetech, LLC, is robust enough to immediately consider using it in large LTD accelerators. The impedance of the arcs in the switch is strongly dependent on the balance of the circuit. When discharged onto a short circuit, the arc impedances were $\sim$0.55 Ohms during the power pulse and 0.15–0.3 Ohms thereafter. When discharged into a matched load, the arc impedances were typically 0.8–1.2 Ohms. Stray capacitances significantly degraded the trigger pulses to the switches in some of these experiments, emphasizing the need to monitor the trigger pulse at the switch.

ACKNOWLEDGMENTS

We are grateful for a number of helpful technical discussions with Dr. J. E. Maenchen, Dr. D. H. McDaniel, Dr. J. J. Leckbee, Dr. M. E. Savage, Dr. M. G. Mazarakis, Dr. P. A. Miller, and Mr. W. E. Fowler at Sandia National Laboratories; Mr. I. A. Smith, Mr. R. White, D. L. Johnson, and E. Neau at L3 Communications, Pulse Sciences; Dr. A. A. Kim at the High Current Electronics Institute in Tomsk; and Mr. J. Ennis and others at General Atomics Corporation. This work was supported by a Laboratory-Directed Research and Development grant from Sandia National Laboratories. Sandia is a multiprogram laboratory operated by Sandia Corporation, a Lockheed-Martin company, for the United States Department of Energy's National Nuclear Security Administration under Contract No. DE-AC04-94AL85000.

[1] F. Lassale, A. Loyen, A. Georges, B. Roques, H. Calamy, C. Mangeant, J. F. Cambonie, S. Laspalles, D. Cadars, G. Rodriguez, J. M. Delchie, P. Combes, T. Chancone, and J. Saves, in *Proceedings of the 16th IEEE Pulsed Power Conference, 2007, Albuquerque, NM* (IEEE, Piscataway, NJ, 2007), pp. 217–220, IEEE Catalog 07CH37864C, ISBN 1-4244-0914-4.

[2] A. A. Kim, A. N. Bastrikov, S. N. Volkov, V. G. Durankov, B. M. Kovalchuk, and V. A. Sinebryukhov, in *Proceedings of 14th IEEE Pulsed Power Conference, Dallas, TX, 2003* (IEEE, Piscataway, NJ, 2007), pp. 853–854, IEEE Catalog 07CH37864C, ISBN 1-4244-0914-4.

[3] J. Leckbee, J. Maenchen, S. Portillo, S. Cordova, I. Molina, D. L. Johnson, A. A. Kim, R. Chavez, and D. Ziska, in *Proceedings of the 15th IEEE Pulsed Power Conference, Monterey, CA, 2005* (IEEE, Piscataway, NJ, 2005), pp. 132–135, IEEE Catalog 07CH37864C, ISBN 1-4244-0914-4.

[4] G. A. Mesyats, *Pulsed Power* (Kluwer Academic/Plenum Publishers, New York, 2005), ISBN 0-306-48653-9, pp. 264–265.

[5] J. J. Leckbee, J. E. Maenchen, D. L. Johnson, S. Portillo, D. E. Van DeValde, D. V. Rose, and B. V. Oliver, IEEE Trans. Plasma Sci. **34**, 1888 (2006).

[6] A. A. Kim, A. N. Bastrikov, S. N. Volkov, V. G. Durakov, B. M. Kovalchuk, and V. A. Sinebryukhov, in *Proceedings of the 13th International Symposium on High Current Electronics, Tomsk Russia, 2004* (High Current Electronics Institute, Tomsk, Russia, 2004), pp. 141–144.

[7] Xuandong Liu, Fengju Sun, Tianxue Liang, Xiaofeng Jiang, Qiaogen Zhang, and Aici Qiu, ''Experimental Study on Synchronous Discharge of Ten Multi Gap Multi Channel Gas Switches,'' IEEE Trans. Plasma Sci. (to be published).

[8] W. A. Stygar, M. E. Cuneo, D. I. Headley, H. C. Ives, R. J. Leeper, M. G. Mazaratis, C. L. Olson, J. L. Porter, T. C. Wagoner, and J. R. Woodworth, Phys. Rev. ST Accel. Beams **10**, 030401 (2007).

[9] E. A. Weinbrecht, D. D. Bloomquist, D. H. McDaniel, D. A. Tabor, J. W. Weed, T. V. Faturos, G. R. McKee, and P. J. Warner, in Proceedings of the 15th IEEE Pulsed Power Conference, Monterey, CA, 2005 (Ref. [3]), pp. 170–173.

[10] D. Johnson, V. Bailey, R. Altes, P. Corcoran, I. Smith, S. Cordova, K. Hahn, J. Maenchen, I. Molina, S. Portillo, E. Puetz, M. Sceiford, D. Van DeValde, D. Rose, B. Oliver, D. Welch, and D. Droemer, in Proceedings of the 15th IEEE Pulsed Power Conference, Monterey, CA, 2005 (Ref. [3]), pp. 314–317.

[11] I. D. Smith, V. L. Bailey, Jr., J. Fockler, J. S. Gustwiler, D. L. Johnson, J. E. Maenchen, and D. W. Droemer, IEEE Trans. Plasma Sci. **28**, 1653 (2000).

[12] J. J. Ramirez, K. R. Prestwich, D. L. Johnson, J. P. Corley, G. J. Dension, J. A. Alexander, T. L. Franklin, J. P. Pankuch, T. W. L. Sanford, T. J. Sheridan, L. L. Torrison, and G. A. Zawadzkas, in *Proceedings of the 7th IEEE Pulsed Power Conference, 1989* (IEEE, Piscataway, NJ, 1989), pp. 26–29, IEEE Catalog 07CH37864C, ISBN 1-4244-0914-4.

[13] K. R. Lechien, M. E. Savage, V. Anaya, D. E. Bliss, W. T. Clark, J. P. Corley, G. Feltz, J. E. Garrity, D. W. Guthrie, K. C. Hodge, J. E. Maenchen, R. Maier, K. R. Prestwich, K. W. Struve, T. Thompson, J. Van Den Avyle, P. E. Wakeland, Z. R. Wallace, and J. R. Woodworth, Phys. Rev. ST Accel. Beams **11**, 060402 (2008).

[14] J. R. Woodworth, J. M. Lehr, J. Elizondo-Decanini, P. A. Miller, P. Wakeland, M. Kincy, J. Garde, B. Aragon, W. Fowler, G. Mowrer, J. E. Maenchen, G. S. Sarkisov, J. Corley, K. Hodge, S. Drennan, D. Guthrie, M. Navarro, D. L. Johnson, H. C. Ives, M. J. Slattery, and D. A. Muirhead, IEEE Trans. Plasma Sci. **32**, 1778 (2004).

[15] P. Sincerny, K. Childers, D. Kortbawi, I. Roth, C. Stallings, J. Riordan, B. Hoffman, L. Schlitt, and C. Myers, in *Proceedings of the 11th IEEE Pulsed Power Conference, 1997* (IEEE, Piscataway, NJ, 1997), pp. 698–701, IEEE Catalog 07CH37864C, ISBN 1-4244-0914-4.

[16] I. A. Smith, Phys. Rev. ST Accel. Beams **7**, 064801 (2004).

[17] B. M. Kovalchuk, A. A. Kim, E. V. Kumpjak, N. V. Zoi, J. P. Corley, K. W. Struve, and D. L. Johnson, in *Proceedings of the 13th IEEE Pulsed Power Conference, Las Vegas, NV, 2001* (IEEE, Piscataway, NJ, 2001), pp. 1739–1742, IEEE Catalog 07CH37864C, ISBN 1-4244-0914-4.

[18] M. G. Mazarakis, W. E. Fowler, A. A. Kim, V. A. Sinebryukhov, S. T. Rogowski, R. A. Sharpe, D. H. McDaniel, C. L. Olson, J. R. Porter, K. W. Struve, W. A Stygar, and J. R. Woodworth, Phys. Rev. ST Accel. Beams 12, 050401 (2009).

[19] A. A. Kim (private communication).

[20] Model 35426 capacitors from General Atomics.

[21] L3 Communications, Pulse Sciences Division, 2700 Merced St., San Leandro, CA 94577.

[22] Model 40264-200.

[23] Model 40264.

[24] General Atomics model 31165 capacitors.

[25] M. Mazarakis (private communication).

[26] W. Fowler (private communication).

[27] S. F. Glover, F. E. White, K. W. Reed, and M. J. Harden, "Genetic Optimization for Pulsed Power System Configuration," IEEE Trans. Plasma Sci. (to be published).

[28] F. E. White, S. F. Glover, K. W. Reed, and M. J. Harden, in Proceedings of the 16th IEEE Pulsed Power Conference, 2007, Albuquerque, NM (Ref. [1]).

[29] J. M. Lehr (private communication).

[30] F. W. Grover, *Inductance Calculations, Working Formulas and Tables* (Dover Publications, Inc., Mineola, NY, 1946), ISBN 0-486-49577-9, p. 35.

[31] R. B. Miller, *An Introduction to the Physics of Intense Charged Particle Beams* (Plenum Press, New York, 1982), ISBN 0-306-40931-3, p. 17.

[32] Model 40230 trigger generator from L3 Communications, Pulse Sciences.

[33] A. Nagaoka, J. Coll. Sci., Imp. Univ. Tokyo **27**, 18 (1909).

[34] F. W. Grover, Inductance Calculations (Ref. [30]), pp. 142–160.